PTEP

Prog. Theor. Exp. Phys. **2021**, 113D02 (11 pages)
DOI: 10.1093/ptep/ptab126

Existence of core excited ^{8}Be* $= \alpha + \alpha^*$ cluster structure in $\alpha + \alpha$ scattering

Yoshiharu Hirabayashi[1,*] and Shigeo Ohkubo[2]

[1]*Information Initiative Center, Hokkaido University, Sapporo 060-0811, Japan*
[2]*Research Center for Nuclear Physics, Osaka University, Ibaraki, Osaka 567-0047, Japan*
*E-mail: hirabay@iic.hokudai.ac.jp

Received June 14, 2021; Revised September 11, 2021; Accepted September 21, 2021; Published October 4, 2021

We show the existence of the $\alpha+\alpha^*$ cluster structure at the highly excited energy around $E_x = 20$ MeV in ^{8}Be for the first time in the coupled-channel calculations. An extended double-folding model derived using a realistic precise cluster wave function with a well-developed $N + 3N$ cluster structure for the first excited state of ^{4}He was employed. The calculation reproduces the experimental phase shifts in $\alpha + \alpha$ scattering up to $E_{\rm c.m.} = 21$ MeV well. The result shows that the well-developed core-excited $\alpha + \alpha^*$ structure appears as resonances for $L = 0$ and 2 near the $\alpha + \alpha^*$ threshold which correspond to the experimental states at $E_x = 20.20$ MeV and $E_x = 22.24$ MeV in ^{8}Be.

Subject Index D11, D20, D22

1. Introduction

The α cluster model was proposed [1–3] soon after the discovery of the neutron [4], before the nuclear shell model [5,6] and the collective model, and was continued in ^{8}Be [7] as the *prototype* [8–11]. The cluster model has been shown to be successful not only in light nuclei [12,13] but also in the medium [14,15] and heavy [16–21] mass ranges. On the other hand, the cluster structure with core excitation has been known widely, for example, such as $\alpha+^{12}$C(0_2^+) [22], $\alpha+^{16}$O(0_2^+) [23], $\alpha+^{40}$Ca(0_2^+) [24], $\alpha+^{208}$Pb(3^-) [25,26] and ^{12}C+^{12}C(2^+) molecular structure [27,28]. However, the existence of the cluster structure with α-core excitation has not been confirmed because of the highly excited states of α, which is the lightest tightly bound magic nucleus.

$\alpha+\alpha$ scattering and its interaction potential have been most thoroughly studied both experimentally [29–32] and theoretically [8–10,33,34]. The phenomenological potential with a repulsive core at around $R = 2$ fm for the orbital angular momentum $L = 0$ and 2 waves was shown to originate from the Pauli principle [8–10]. On the other hand, the systematic and unified study of anomalous large angle scattering (ALAS), pre-rainbow and rainbow scattering and cluster structure in the bound and quasi-bound energy region for the typical $\alpha+^{16}$O, $\alpha+^{40}$Ca and ^{16}O+^{16}O systems has shown that the interaction potentials are deep [35–45] due to the Pauli principle [46]. A deep potential has been considered to be favored for the prototype $\alpha + \alpha$ system [46,47], although ALAS and/or rainbows have not been observed clearly and typically because of the lightest double-closed identical boson system. The phenomenological potentials with a repulsive core for $\alpha + \alpha$, such as in Ref. [48], which has been widely used historically, is now understood as a mathematically supersymmetric partner [49] of the deep potential such as in Ref. [47].

Although the potential for $\alpha + \alpha$ has been established, it is to be noted that the experimental phase shifts are reproduced successfully only at the low energy region below $E_L = 40$ MeV where inelastic

channels are closed [33]. Above $E_L = 42.4$ MeV, where inelastic channels open, the experimental phase shifts with a non-smooth complicated structure have not been explained. The coupled-channel $\alpha + \alpha^*$ calculations, assuming a monopole vibration for the first excited state 0_2^+ of ^{4}He, were attempted as early as in the 1970s [50,51]. An experimental search for the cluster structure $\alpha + \alpha^*$ was also done [52,53]. However, the existence of the $\alpha + \alpha^*$ cluster structure has not been confirmed.

The structure of ^{8}Be at the highly excited energy region has also had attention paid to it from the viewpoint of the cosmological lithium problem [54,55]. One of the candidates to reduce the ^{7}Li abundance is the ^{7}Be$(n,\alpha)\alpha$ reaction, and the ^{7}Be+n channel is opened as an highly excited state of ^{8}Be at $E_x = 18.899$ MeV. Because the direct ^{7}Be$(n,\alpha)\alpha$ breakup channel is strongly suppressed and the ^{7}Be$(n,\gamma\alpha)\alpha$ reaction remains the dominant process, the highly excited states of ^{8}Be may affect the reaction corresponding the α-emitting cross section of these states [54].

The purpose of this paper is to show the existence of the $\alpha + \alpha^*$ structure as a prototype of α–core excited cluster structure for the first time, in which α is excited to the 0_2^+ state at 20.21 MeV, analyzing $\alpha + \alpha$ scattering using the coupled-channel method with an extended double-folding model derived from the precise wave functions for ^{4}He. We also show how the α cluster structure appears at a highly excited energy region near the $\alpha + \alpha^*$ threshold. The paper is organized as follows. In Sect. 2 the extended double-folding model is presented. Sect. 3 is devoted to the coupled-channel analysis of $\alpha + \alpha$ scattering and the core excited $\alpha + \alpha^*$ cluster structure in ^{8}Be. In Sect. 4 the core excited α cluster structure in ^{8}Be is discussed. Our conclusion is given in Sect. 5.

2. The extended double-folding model

An extended double-folding model that describes all the diagonal and off-diagonal coupling potentials derived from the microscopic realistic precise wave functions for ^{4}He is given as follows:

$$V^N_{ij,kl}(\mathbf{R}) = \int \rho^{(^4\mathrm{He})}_{ij}(\mathbf{r}_1)\rho^{(^4\mathrm{He})}_{kl}(\mathbf{r}_2)v_{NN}(\mathbf{r}_1 + \mathbf{R} - \mathbf{r}_2)d\mathbf{r}_1 d\mathbf{r}_2, \tag{1}$$

where $\rho^{(^4\mathrm{He})}_{ij}(\mathbf{r})$ is the diagonal ($i = j$) or transition ($i \neq j$) nucleon density of ^{4}He calculated in the microscopic four-body calculations in Ref. [56]. In the coupled-channel calculations we take into account the 0_1^+ (0.0 MeV) and 0_2^+ (20.21 MeV) states of ^{4}He. For the effective two-body interaction v_{NN} we use the M3Y interaction [57]. We introduce a normalization factor, N_R. The Coulomb folding potential $V^C_{ij,kl}(\mathbf{R})$ is similarly calculated in the folding model of Eq. (1) by replacing v_{NN} by v_{Coul}.

3. Analysis of $\alpha + \alpha$ scattering and $\alpha + \alpha^*$ cluster structure

In Fig. 1(a) the calculated phase shifts for $L = 0$, 2 and 4 in $\alpha + \alpha$ scattering calculated using the coupled-channel method (solid lines) with a double-folding model are compared with the experimental data [32]. Although $N_R = 0.999943$ is used to reproduce the experimental ground state energy of 91.84 keV from the $\alpha + \alpha$ threshold and the α decay width 5.57 eV of ^{8}Be [58] where calculated values are 91.84 keV and 5.5 eV, the calculated phase shifts, cross sections and the discussions that come up later are not very sensitive to this fine adjustment. The results calculated in the single channel by switching off the coupling (dashed lines) are also displayed for comparison. The behavior of the experimental phase shifts for $L = 0$, 2 and 4 at $E_{\mathrm{c.m.}} < 20$ MeV is reproduced well by the calculations. What is noticeable in Fig. 1(a) is that the kinks at around $E_{\mathrm{c.m.}} = 20$ MeV in the experimental data, which cannot be reproduced in the single-channel calculations [47], are also seen in the present coupled-channel calculations. Thus the kinks are found to arise from the coupling to the excited 0_2^+ state of ^{4}He. The calculations give no kink for $L = 4$ at around $E_{\mathrm{c.m.}} = 20$ MeV.

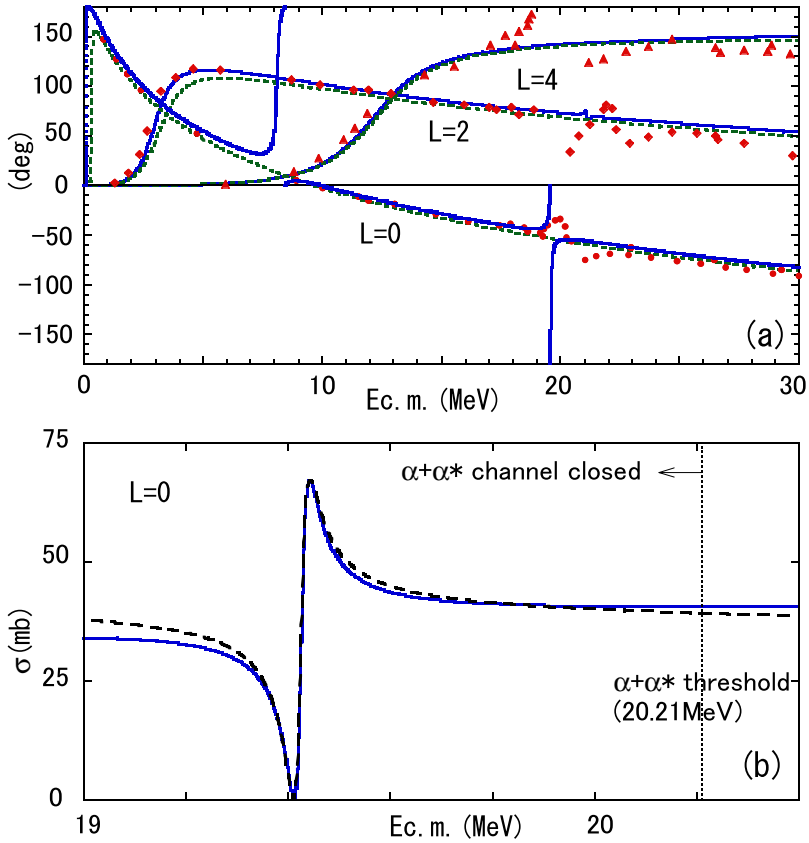

Fig. 1. (a) The phase shifts in $\alpha + \alpha$ scattering calculated using the coupled-channel method (solid lines) and in the single channel (dashed lines) with a double-folding model are compared with the experimental data for $L = 0$ (circles), $L = 2$ (diamonds) and $L = 4$ (triangles) taken from Ref. [32]. (b) The calculated elastic $\alpha + \alpha$ scattering cross section for $L = 0$ resonance just below the threshold energy (solid line). The dashed line shows a fit by a Fano profile.

The irregular behavior of the calculated phase shift at around $E_{\rm c.m.} = 8$ MeV is the redundant Pauli forbidden $0s$ state in the $\alpha + \alpha^*$ channel, as discussed later.

Fig. 1(b) shows the resonance behavior of the cross section at around $E_{\rm c.m.} = 20$ MeV for $L = 0$ due to the s-wave coupling to the $J = 0^+$ resonance with the $\alpha + \alpha^*$ cluster structure in ^{8}Be. It shows a closed channel resonance (Feshbach resonance) [59–61] below the $\alpha + \alpha^*$ threshold, in which the relative kinetic energy between two α particles is negative due to the loss of its energy by the excitation of α to the 0^+_2 state, and the wave function of the excited $\alpha + \alpha^*$ state shows an exact bound state nature without scattering amplitudes at large distance (see Fig. 5a). The calculated resonance behavior of the cross section can be well reproduced by the Fano resonance [62,63] formula (Fano profile),

$$\sigma(E_{\rm c.m.}) = [4\pi(2L+1)]\,\frac{(\varepsilon+q)^2}{k^2(1+q^2)(1+\varepsilon^2)},$$
$$\varepsilon = \frac{E_{\rm c.m.} - E_{\rm res}}{\Gamma/2},\ q = -\cot\delta_b, \tag{2}$$

where k and δ_b are the wave number of relative motion between two α particles and the background phase at the resonance energy, respectively. This formula is reduced to the Breit–Wigner formula [64] in a limit of $\delta_b = 0$. We take $\delta_b = -50.0°$ (see Fig. 1a), the resonance energy $E_{\rm res} = 19.425$ MeV

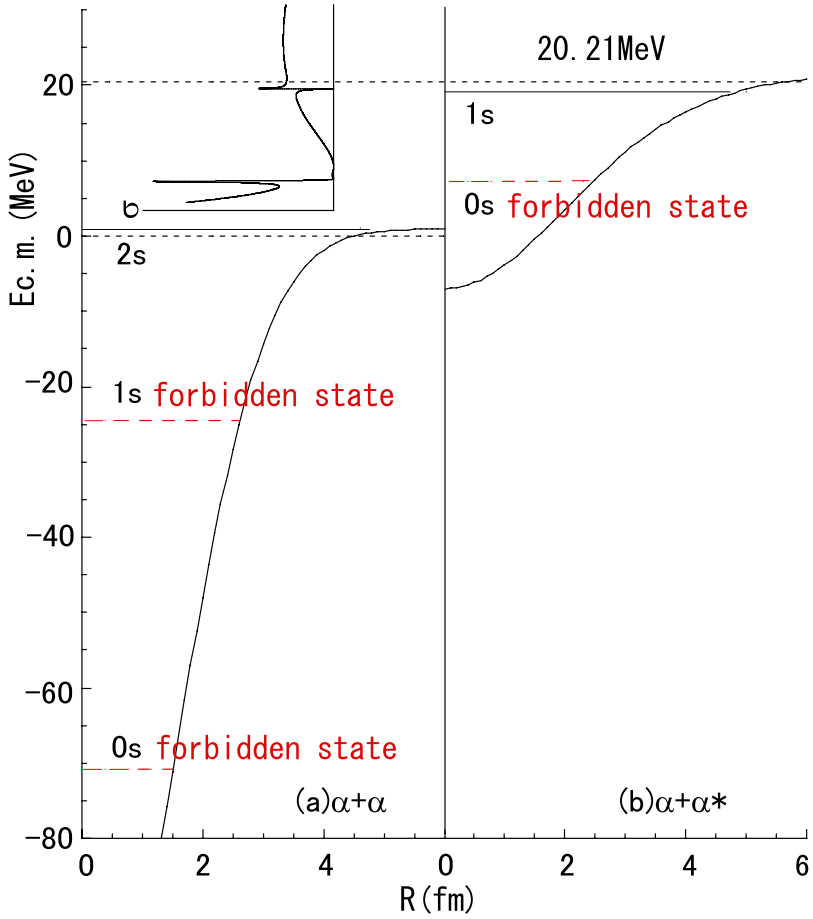

Fig. 2. The calculated diagonal double folding potentials for the (a) $\alpha + \alpha$ and (b) $\alpha + \alpha^*$ channels together with the embedded Pauli forbidden states (red dashed horizontal lines), $0s$ and $1s$ in (a) and $0s$ in (b) for $L = 0$, and the threshold energies (black dashed horizontal lines) are displayed. The Pauli allowed physical states calculated in the coupled-channel method (solid horizontal lines), $2s$ in (a) and $1s$ in (b), and the elastic scattering cross section (σ) for $L = 0$ (the solid curve) are also shown.

and the width parameter $\Gamma = 32$ keV(dashed line). In Fig. 1(b), the calculated cross section shows a typical Fano resonance and the asymmetric shape comes from the interference between the elastic channel as a background continuum state and the 0_2^+ channel as a discrete excited state. Although the α width seems to be small compared with the experimental 0_2^+ state of ^{8}Be at $E_x = 20.20$ MeV with the width about 350 keV [53,58], it may be due to the effect of the open channels such as p+^{7}Li and n+^{7}Be in ^{8}Be which are not taken into account in the present coupled-channel calculations. The coupling with states at higher energies such as the 1^- ($T = 0$) at 24.250 MeV, which has a well-developed N+3N structure as a parity doublet partner [65] of the 0_2^+ state at 20.210 MeV of ^{4}He, is also not included in the present framework. These states could be an origin of the wiggles in the highly excited states. A more involved coupled-channel calculation including higher excited states would be a future subject of study. On the other hand, the positions of the resonance energy are rather sensitive to the strength of the coupling potential.

In Fig. 2 the diagonal potentials for the $\alpha + \alpha$ and $\alpha + \alpha^*$ channels are displayed. The diagonal nuclear potential for the $\alpha + \alpha$ channel is similar to that in Ref. [47]. This potential accommodates the deeply bound redundant Pauli forbidden $0s$ and $1s$ states for $L = 0$ (Fig. 2a) and the $0d$ state

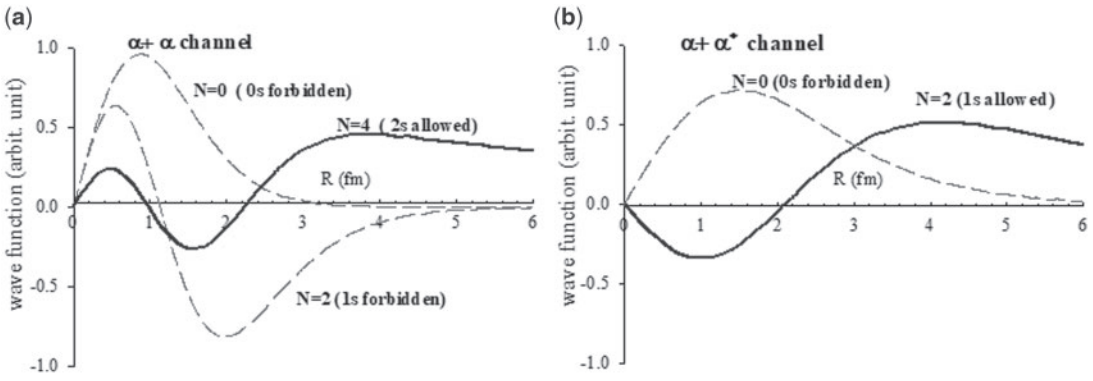

Fig. 3. The relative wave functions (multiplied by R) for $L = 0$ of the redundant Pauli forbidden state (red dashed lines) and the Pauli allowed states (blue solid lines) calculated in the bound state approximation for the $\alpha + \alpha$ and the $\alpha + \alpha^*$ channels with the diagonal potentials in Fig. 2.

for $L = 2$. The Pauli forbidden states play a role in damping the amplitudes of the physical wave functions in the internal region, $R < 2$ fm, which corresponds to the core radius of the L-dependent shallow potential with a repulsive core in Refs. [8–10]. The gross behavior of the phase shifts is essentially reproduced by the diagonal $\alpha + \alpha$ potential. The potential for $\alpha + \alpha^*$ is shallow, with its strength being about a quarter of the $\alpha + \alpha$ potential at $R = 0$ fm (Fig. 2b) and is extended much to the outer region reflecting the $N + 3N$ cluster structure of the 0_2^+ state of ^{4}He. This potential accommodates the redundant Pauli forbidden $0s$ state at -12.7 MeV, $E_{\text{c.m.}} = 8$ MeV, from the $\alpha + \alpha^*$ threshold energy for $L = 0$ (Fig. 2b).

In order to make it easier to understand the physical meaning of the Pauli allowed physical states and their scattering state wave functions solved in the coupled-channel method, which will be discussed in Fig. 4 and Fig. 5, we show in Fig. 3 both the Pauli forbidden and allowed wave functions of the relative motion for $L = 0$, calculated in the bound state approximation in the single channel using the $\alpha + \alpha$ potential and the $\alpha + \alpha^*$ potential. In the $\alpha + \alpha$ channel the Pauli allowed physical states should satisfy the Wildermuth condition $N = 2n + L = 4$ with n being the number of the nodes in the relative wave function. For the $\alpha + \alpha^*$ channel the physical states should satisfy the Wildermuth condition $N = 2$. The number of the nodes in the Pauli allowed wave functions in Fig. 3 solved in the bound state approximation satisfies the Wildermuth condition. For the $\alpha + \alpha$ channel the Pauli allowed wave function has two nodes with the outermost node at around 2 fm, which is the well-known energy independent node discovered in Refs. [8,9] and corresponds to the radius of the repulsive core potential for $L = 0$. For the $\alpha + \alpha^*$ channel the wave function of the Pauli allowed 0^+ state has only one node at around 2 fm, which is also energy-independent due to the Pauli principle.

The shallow and extended properties of the potential for the $\alpha + \alpha^*$ channel in Fig. 2 are understood naturally from the wave function of the ^{4}He(0_2^+) state. This state at $E_x = 20.210$ MeV with 100% p-decay width [58] is located 0.396 MeV above the $p+^3$H threshold (19.814 MeV) and 0.368 MeV below the $n+^3$He threshold (20.578 MeV) and has been shown to have the $N + 3N$ cluster structure [56,66]. The calculated rms radius, 3.16 fm in Ref. [66] and 4.2 fm in Ref. [56], is much larger than that of the ground state of ^{4}He, 1.63 fm. This is very large even compared with the calculated size, 3.2–3.8 fm [67–75] of the well-developed gas-like dilute three α cluster 0_2^+ Hoyle state in ^{12}C at $E_x = 7.654$ MeV, located 0.287 MeV above the α threshold energy.

To see the underlying structure in the kink of the phase shift at around $E_{\text{c.m.}} = 21$ MeV for $L = 2$ seen in Fig. 1, the calculated elastic scattering cross section, the Argand diagram, and the calculated

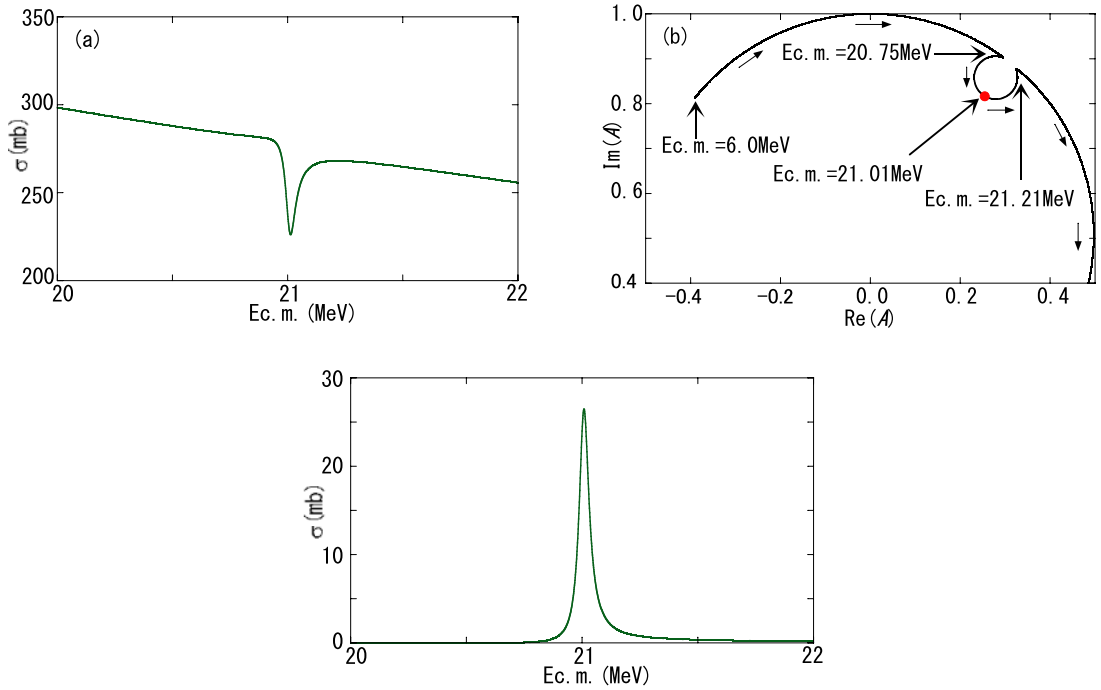

Fig. 4. (a) The calculated elastic $\alpha + \alpha$ scattering cross section between $E_{\rm c.m.} = 20$ and 22 MeV for $L = 2$, (b) the Argand diagram $A = (S_L - 1)/2i$ for $L = 2$, with S_L being the elastic scattering S matrix and (c) the calculated inelastic scattering cross section to the 0_2^+ channel for $L = 2$.

inelastic cross section to the 0_2^+ channel are displayed in Fig. 4. We see a dip at $E_{\rm c.m.} = 21.01$ MeV in the elastic scattering cross section (Fig. 4a). This is related to the existence of the 2^+ resonance in the $\alpha + \alpha^*$ channel. Although the elastic cross section does not show a Breit–Wigner type behavior of resonance because the phase shift does not pass through 90°, the resonant nature can be confirmed by looking into the Argand diagram [76–78]. As seen in Fig. 4(b), the diagram of the elastic channel exhibits a rapid counterclockwise change of the phase as a function of energy at $E_{\rm c.m.} = 21.01$ MeV, which is the signature of a resonance in the coupled channels system. As a side note, the point where the Argand loop crosses the vertical axis from right to left with increasing energy corresponds to the phase shift of 90° in the case without coupled-channel effects. It is to be noted, however, that the Argand loop does not generally imply the existence of a resonance unless a peak in the cross section is accompanied [76,77]. Our calculated cross section to the 0_2^+ channel for $L = 2$ in Fig. 4(c) clearly shows a sharp peak at this energy. Thus it is found that an $L = 2$ resonance occurs at $E_{\rm c.m.} = 21.01$ MeV *above* the $\alpha + \alpha^*$ threshold as a molecular resonance [27,28] with the centrifugal barrier. In this molecular 2^+ state, the calculated mixing probabilities inside $R = 4.5$ fm are 99.76% for the $\alpha + \alpha^*$ component and 0.24% for the $\alpha + \alpha$ component.

The experimental 0^+ state at $E_x = 20.20$ MeV ($\Gamma = 0.720$ MeV) and the 2^+ state at 22.24 MeV ($\Gamma \sim 0.8$ MeV) in ^{8}Be [58] correspond well to the calculated 0^+ state at $E_{\rm c.m.} = 19.45$ MeV and 2^+ state at $E_{\rm c.m.} = 21.01$ MeV, respectively. That is, they have the $\alpha + \alpha^*$ cluster structure.

The emergence of the resonances in the $\alpha + \alpha^*$ channel can be confirmed in another way by investigating the drastic changes of the wave functions with $E_{\rm c.m.}$ in the vicinity of the resonance energy. In Figs. 5(b) and 5(c) the wave functions in the *elastic* channel for $L = 0$ at around $E_{\rm c.m.} = 19.45$ MeV calculated via the coupled-channel method are displayed as a function of $E_{\rm c.m.}$ from 19.35 MeV to 19.50 MeV in a small step. As the energy increases from $E_{\rm c.m.} = 19.35$ MeV to 19.41

MeV, the first node at around $R = 1$ fm moves outward, while the position of the second node at $R = 2$ fm is almost energy-independent, which is due to the orthogonality to the forbidden $0s$ and $1s$ states in the $\alpha + \alpha$ channel indicated in Fig. 2(a). The Wildermuth condition $N = 4$ is satisfied for these wave functions. What is to be noticed is that at 19.44, 19.45 and 19.46 MeV no node appears at around $R = 1$ fm and the first node appears at $R = 2$ fm, which means that at these energies the wave functions no longer satisfy the Wildermuth condition $N = 4$ for the *elastic* channel; that is, the wave functions seem to disappear from the $\alpha + \alpha$ channel. In fact, the calculated mixing probability inside $R = 4.5$ fm at resonance energy 19.45 MeV shows the dominant $\alpha + \alpha^*$ component (99.82%) while the $\alpha + \alpha$ component is negligibly small, 0.18%. The wave functions at 19.44 and 19.45 MeV are out of phase at around $R = 3$ fm with those at the lower energies 19.35, 19.38 and 19.41 MeV as shown in Fig. 5(b). At 19.48 MeV, the first node appears again at $R = 0.6$ fm and the second node remains at the energy-independent $R = 2$ fm, thus again appears in the $\alpha + \alpha$ channel. The energy interval between 19.435 MeV and 19.465 MeV, where the first node disappears, apparently violating the Wildermuth condition in the $\alpha + \alpha$ channel, corresponds to the width of the resonance at $E_{\rm c.m.} = 19.45$ MeV. In Fig. 5(a) the wave function of the inelastic channel as well as that of the elastic channel on the resonance energy 19.45 MeV is shown. It should be noted that the number of the node satisfies $N = 2$ on this resonance energy although $N = 4$ is satisfied at other energies, that is, the number of node is *decreased* on the resonance. We see that the former has the first node at $R = 2$ fm, satisfying the Wildermuth condition in the inelastic channel, and the latter has the first node at $R = 2$ fm, violating the Wildermuth condition in the elastic channel. The inelastic channel wave function is much extended to 8 fm, reflecting that it has the $\alpha + \alpha^*(3N + N)$ structure.

In Fig. 5(a) the first node of the inelastic scattering wave function at 19.45 MeV, which appears near $R = 2$ fm, is very close to that of the $N = 2$ wave function in Fig. 3(b) in the $\alpha + \alpha^*$ channel solved in the bound state approximation. This shows that in the resonance energies where the Wildermuth condition in the $\alpha + \alpha$ channel does not apparently work, the inelastic wave function satisfies the $N = 2$ Wildermuth condition in the $\alpha + \alpha^*$ channel, being orthogonal to the redundant Pauli forbidden $0s$ state indicated in Fig. 2(b). This is understood by looking into the properties of the kink in the phase shift of $L = 0$ at $E_{\rm c.m.} = 8.1$ MeV in Fig. 1. From the changes of the wave functions with energy in the vicinity of $E_{\rm c.m.} = 8.1$ MeV, which is very similar to the behavior seen in Fig. 5, it is found that this kink is the redundant $0s$ Pauli forbidden state in the $\alpha + \alpha^*$ channel in Fig. 2(b). Thus the Paul forbidden states in both the $\alpha + \alpha$ and $\alpha + \alpha^*$ channels are correctly incorporated in the present deep potential. The forbidden states in the $\alpha + \alpha$ channel for $L = 0$ and 2 are in the deeply bound region, and the $0s$ forbidden state in the $\alpha + \alpha^*$ channel for $L = 0$ is also in the deeply bound region below the $\alpha + \alpha^*$ threshold. Since the solved physical $L = 0$ state with the $\alpha + \alpha^*$ structure is exactly orthogonal to this Pauli forbidden state, the present model calculations are a mimic of Saito's orthogonality condition model [79,80]. On the other hand, for $L = 2$ state there is no forbidden state in the $\alpha + \alpha^*$ channel.

4. Discussion

We discuss why a state with the $\alpha + \alpha^*$ structure in ^{8}Be was not obtained in the microscopic coupled-channel calculations using the resonating group method in Ref. [51] where none of the calculated phase shifts for $L = 0,\ 2$, and 4 as well as $L = 1$ and $L = 3$ pass through 90°. This is probably because the wave function for the ^{4}He(0_2^+) state was not appropriate since the monopole vibration state was assumed. In fact, the precise wave function for ^{4}He(0_2^+) we used has a very extended

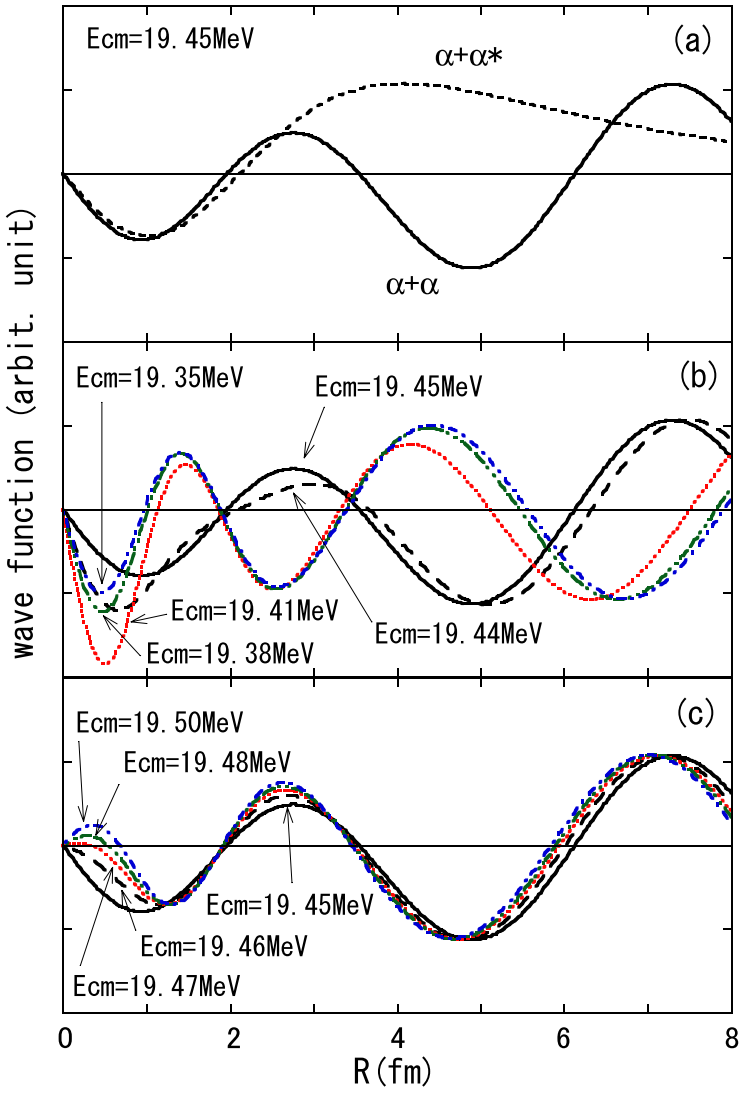

Fig. 5. (a) The calculated scattering wave functions (multiplied by R) for the elastic and inelastic channels on the resonance energy $E_{\text{c.m.}} = 19.45$ MeV for $L = 0$. The wave functions in the elastic channel in the vicinity of the resonance energy show the drastic changes of the number of the nodes and the nodal position *below* (b) and *above* (c) the resonance energy.

$N + 3N$ cluster structure, which is essential in causing a strong coupling between the $\alpha + \alpha$ and the $\alpha + \alpha^*$ channels.

In Fig. 6 the energy levels with the $\alpha + \alpha$ and the $\alpha + \alpha^*$ cluster structure obtained in the present calculations are compared with the experimental energy levels and the energy levels calculated using the tensor-optimized shell model (TOSM) with the AV8' force and the Minnesota force [81] and the Monte Carlo calculations [82]. The present calculation reproduces not only the experimental energy levels of the ground band but also the highly excited 0_2^+ and 2_2^+ states well. On the other hand, the shell model calculations locate the first excited 0^+ state considerably lower than the experimental energy level. Although the structure of this 0^+ state is not discussed in Ref. [81], it could correspond to the 0^+ state with the $\alpha + \alpha^*$ cluster structure if the shell model space is enlarged sufficiently. In the *ab initio* calculations, Wiringa et al. [82] got no highly excited $J = 0^+, 2^+$ states with $T = 0$

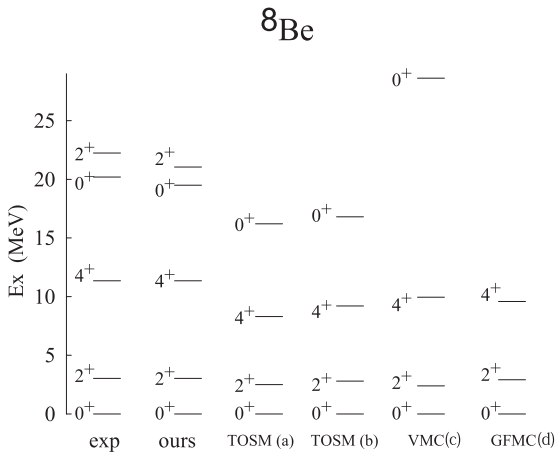

Fig. 6. The energy levels of ^{8}Be of the experimental data [58], the present coupled channels α cluster model calculations and the tensor-optimized shell model calculations [81], TOSM (a) with the AV8' force and TOSM (b) with the Minnesota force, and (c) variational Monte Carlo calculation and (d) Green's function Monte Carlo calculation[82], are compared.

in the Green's function Monte Carlo calculations and a 0^+_2 at 28.62 MeV in the variational Monte Carlo calculations, which is far from the experimental 0^+_2 state.

The rotational constant $k = \hbar^2/2\mathcal{J} = 0.25$ MeV, with $\mathcal{J}$ being the moment of inertia, of the $\alpha + \alpha^*$ cluster band estimated from the experimental states shows that the moment of inertia of the band is about twice as large as that of the ground band with $k = 0.57$ MeV. This large moment of inertia is reasonable considering that the α^* has a very extended $N + 3N$ cluster structure, as seen in Fig. 5(a), where the wave function of the 0^+_2 state is extremely extended up to more than 8 fm with the dilute density distribution compared with the $\alpha + \alpha$ cluster structure of the ground state 0^+. We note that this band is very similar in extended nature to the $K = 0^+_2$ band with $k = 0.28$ built on the Hoyle state at 7.65 MeV in ^{12}C [73,83] and the $K = 0^+$ band at 16.7 MeV in ^{16}O with very large moment of inertia, $k = 0.064$ MeV in Ref. [84] and $k = 0.095 \pm 0.020$ MeV in Ref. [85] with the dilute α+^{12}C (0^+_2; 7.65 MeV) structure [22,86].

The present $\alpha + \alpha^*$ cluster picture of the second 0^+ state seems to be supported in a microscopic three-cluster model calculation in Ref. [87], which locates a 0^+_2 state located at 1.44 MeV above the p+ ^{7}Li threshold (18.254 MeV), although its cluster character is not discussed in detail. The present results make an impact on the cluster structure study in nuclei by reinforcing the importance of the concept of core excitation in the lightest nuclei, which has been known in medium-weight and heavy nuclei. Also, as for the ^{7}Be(n,^{4}He)^{4}He reaction, it would be intriguing to investigate the incident energy dependence of the cross sections including the coupling to the $\alpha + \alpha^*$ channel at 20.2 MeV of ^{8}Be.

5. Conclusion

We have studied the $\alpha + \alpha^*$ cluster structure at the highly excited energy in ^{8}Be in the coupled-channel calculations using the double-folding model derived from the precise cluster wave function for the first excited state of ^{4}He(0^+_2). We found that the well-developed core-excited $\alpha + \alpha^*$ structure appears near the $\alpha + \alpha^*$ threshold as a closed channel resonance (Feshbach resonance) for $L = 0$ and a molecular resonance for $L = 2$ which correspond to the experimental states at $E_x = 20.20$ MeV

and $E_x = 22.24$ MeV in ^{8}Be, respectively. The present coupled-channel cluster model approach, which has been powerful for the cluster structure study with core excitation such as the $\alpha+^{40}\mathrm{Ca}^*(0_2^+)$ [24], $\alpha+^{16}\mathrm{O}^*(0_2^+)$ [23] and $\alpha+^{12}\mathrm{C}^*(0_2^+)$ [22] systems, is again found to be powerful for the lightest *prototype* $\alpha+\alpha^*$ cluster structure with α-core excitation in ^{8}Be.

Acknowledgements

The authors are grateful to Prof. M. Kamimura for valuable discussions and providing the transition densities in Ref. [56] in the tabulated form. Y.H. would like to thank Prof. T. Harada for valuable discussions. S.O. expresses sincere thanks to the late Prof. D. M. Brink for interest and encouragement. They thank the Yukawa Institute for Theoretical Physics, Kyoto University for the hospitality extended during a stay in 2018 and 2019.

References

[1] W. Wefelmeier, Z. Phys. **107**, 332 (1937).
[2] J. A. Wheeler, Phys. Rev. **52**, 1083 (1937).
[3] J. A. Wheeler, Phys. Rev. **52**, 1107 (1937).
[4] J. Chadwick, Proc. Royal Soc. A **136**, 692 (1932).
[5] M. G. Mayer, Phys. Rev. **75**, 1969 (1949).
[6] O. Haxel, J. H. D. Jensen, and H. E. Suess, Phys. Rev. **75**, 1766 (1949).
[7] K. Sekine, M. Taketani, T. Toyoda, and K. Inoue, Soryushiron Kenkyu (Kyoto) **11**, 195 (1956).
[8] I. Shimodaya, R. Tamagaki, and H. Tanaka, Prog. Theor. Phys. **27**, 793 (1962).
[9] R. Tamagaki and H. Tanaka, Prog. Theor. Phys. **34**, 191 (1965).
[10] R. Tamagaki, Prog. Theor. Phys. Suppl. **E68**, 242 (1968).
[11] J. Hiura and R. Tamagaki, Prog. Theor. Phys. Suppl. **52**, 25 (1972).
[12] K. Ikeda, T. Marumori, R. Tamagaki, and H. Tanaka, Prog. Theor. Phys. Suppl. **52**, 1 (1972).
[13] K. Ikeda, H. Horiuchi, and S. Saito, Prog. Theor. Phys. Suppl. **68**, 1 (1980).
[14] S. Ohkubo, M. Fujiwara, and P. E. Hodgson, Prog. Theor. Phys. Suppl. **132**, 1 (1998).
[15] S. Ohkubo, T. Yamaya, and P. E. Hodgson, Nuclear clusters, in *Nucleon-Hadron Many-Body Systems*, ed. H. Ejiri and H. Toki (Oxford University Press, Oxford, 1999), p. 150.
[16] F. Hoyler, P. Mohr, and G. Staudt, Phys. Rev. C **50**, 2631 (1994).
[17] S. Ohkubo, Phys. Rev. Lett. **74**, 2176 (1995).
[18] B. Buck, A. C. Merchant, and S. M. Perez, Phys. Rev. Lett. **72**, 1326 (1994).
[19] S. Okabe, J. Phys. Soc. Japan Suppl. **58**, 516 (1989).
[20] K. Varga, R. G. Lovas, and R. J. Liotta, Phys. Rev. Lett. **69**, 37 (1992).
[21] R. G. Lovas, R. J. Liotta, A. Insolia, K. Varga, and D. S. Delion, Phys. Rep. **294**, 265 (1998).
[22] S. Ohkubo and Y. Hirabayashi, Phys. Lett. B **684**, 127 (2010).
[23] Y. Hirabayashi and S. Ohkubo, Phys. Rev. C **88**, 014314 (2013).
[24] S. Ohkubo, Y. Hirabayashi, and T. Sakuda, Phys. Rev. C **57**, 2760 (1998).
[25] A. Astier, P. Petkov, M.-G. Porquet, D. S. Delion, and P. Schuck, Phys. Rev. Lett. **104**, 042701 (2010).
[26] Y. Suzuki and S. Ohkubo, Phys. Rev. C **82**, 041303(R) (2010).
[27] B. Imanishi, Phys. Lett. B **27**, 267 (1968).
[28] B. Imanishi, Nucl. Phys. A **125**, 33 (1969).
[29] H. E. Conzett, G. Igo, H. C. Shaw, and R. J. Slobodrian, Phys. Rev. **117**, 1075 (1960).
[30] G. Lgo, Phys. Rev. **117**, 1079 (1960).
[31] P. Darriulat, G. Igo, H. G. Pugh, and H. D. Holmgren, Phys. Rev. **137**, B315 (1965).
[32] A. D. Bacher, F. G. Resmini, H. E. Conzett, R. de Swiniarski, H. Meiner, and J. Ernst, Phys. Rev. Lett. **29**, 1331 (1972).
[33] F. Tanabe, A. Tohsaki, and R. Tamagaki, Prog. Theor. Phys. **53**, 677 (1975).
[34] S. Elhatisari, D. Lee, G. Rupak, E. Epelbaum, H. Krebs, T. A. Lähde, T. Luu, Ulf-G. Meißner, Nature **528**, 111 (2015).
[35] D. M. Brink, *Semi-classical Methods for Nucleus-Nucleus Scattering* (Cambridge University Press, Cambridge, 1985).
[36] S. Ohkubo, Y. Kondō, and S. Nagata, Prog. Theor. Phys. **57**, 82 (1977).
[37] F. Michel, J. Albinski, P. Belery, Th. Delbar, Gh. Grégoire, B. Tasiaux, and G. Reidemeister, Phys. Rev. C **28**, 1904 (1983).

[38] Th. Delbar et al., Phys. Rev. C **18**, 1237 (1978).
[39] F. Michel, G. Reidemeister, and S. Ohkubo, Phys. Rev. Lett. **57**, 1215 (1986).
[40] F. Michel, G. Reidemeister, and S. Ohkubo, Phys. Rev. C **37**, 292 (1988).
[41] S. Ohkubo, Phys. Rev. C **38**, 2377 (1988).
[42] E. Stiliaris, H. G. Bohlen, P. Fröbrich, B. Gebauer, D. Kolbert, W. von Oertzen, M. Wilpert, and Th. Wilpert, Phys. Lett. B **223**, 291 (1989).
[43] D. T. Khoa, W. von Oertzen, H. G. Bohlen, and S. Ohkubo, J. Phys. G: Nucl. Part. Phys. **34**, R111 (2007).
[44] F. Michel, S. Ohkubo, and G. Reidemeister, Prog. Theor. Phys. Suppl. **132**, 7 (1998).
[45] S. Ohkubo and K. Yamashita, Phys. Rev. C **66**, 021301(R) (2002).
[46] S. Ohkubo, Phys. Rev. C **93**, 041303(R) (2016).
[47] B. Buck, H. Friedrich, and C. Wheatley, Nucl. Phys. A **275**, 246 (1977).
[48] S. Ali and A. R. Bodmer, Nucl. Phys. **80**, 99 (1966).
[49] D. Baye, Phys. Rev. Lett. **58**, 2738 (1987).
[50] Le-Chi- Niem, P. Heiss, and H. H. Hackenbroich, Z. Phys. **244**, 346 (1971).
[51] H. H. Hackenbroich, T. H. Seligman, W. Zahn, and D. Fick, Phys. Lett. B **62**, 121 (1976).
[52] R. E. Warner, G. C. Ball, W. G. Davies, A. J. Ferguson, and J. S. Forster, Phys. Rev. C **19**, 293(R) (1979).
[53] R. Čaplar, H. Gemmeke, L. Lassen, W. Weiss, and D. Fick, Nucl. Phys. A **342**, 71 (1980).
[54] M. Barbagallo et al. [n_TOF Collaboration], Phys. Rev. Lett. **117**, 152701 (2016).
[55] T. Kawabata et al., Phys. Rev. Lett. **118**, 052701 (2017).
[56] E. Hiyama, B. F. Gibson, and M. Kamimura, Phys. Rev. C **70**, 031001(R) (2004).
[57] G. Bertsch, J. Borysowicz, H. McManus, and W. G . Love, Nucl. Phys. A **284**, 399 (1977).
[58] Brookhaven National Nuclear Data Center. *Evaluated Nuclear Structure File Search and Retrieval* (NNDC, Brookhaven, June 1, 2021) (available at http://www.nndc.bnl.gov/ensdf/, date last accessed)
[59] H. Feshbach, Ann. Phys. **5**, 357 (1958).
[60] H. Feshbach, Ann. Phys. **19**, 287 (1962).
[61] H. Feshbach, *Theoretical Nuclear Physics* (Wiley, New York, 1992).
[62] U. Fano, Nuovo Cimento **12**, 154 (1935).
[63] U. Fano, Phys. Rev. **124**, 1866 (1961).
[64] G. Breit and E. Wigner, Phys. Rev. **49**, 519 (1936).
[65] W. Horiuchi and Y. Suzuki, Phys. Rev. C **78**, 034305 (2008).
[66] H. Furutani, H. Horiuchi, and R. Tamagaki, Prog. Theor. Phys. **60**, 307 (1978).
[67] E. Uegaki, S. Okabe, Y. Abe, and H. Tanaka, Prog. Theor. Phys. **57**, 1262 (1977).
[68] E. Uegaki, Y. Abe, S. Okabe, and H. Tanaka, Prog. Theor. Phys. **62**, 1621 (1979).
[69] Y. Fukushima and M. Kamimura, J. Phys. Soc. Japan Suppl. **44**, 225 (1978).
[70] M. Kamimura, Nucl. Phys. A **351**, 456 (1981).
[71] H. Matsumura and Y. Suzuki, Nucl. Phys. A **739**, 238 (2004).
[72] Y. Kanada-En'yo, Prog. Theor. Phys. **117**, 655 (2007).
[73] Y. Nakamura, J. Takahashi, Y. Yamanaka, and S. Ohkubo, Phys. Rev. C **94**, 014314 (2016).
[74] Y. Nakamura, J. Takahashi, Y. Yamanaka, and S. Ohkubo, Phys. Rev. C **98**, 049901(E) (2018).
[75] R. Katsuragi, K. Kazama, J. Takahashi, Y. Nakamura, Y. Yamanaka, and S. Ohkubo, Phys. Rev. C **98**, 044303 (2018).
[76] K. Langanke and D. Frekers, Nucl. Phys. A **302**, 134 (1978).
[77] N. Masuda, Phys. Rev. D **1**, 2565 (1970).
[78] G. R. Plattner, *Lecture Notes in Physics*, (Springer, Berlin, 1974), Vol. 30, p. 162.
[79] S. Saito, Prog. Theor. Phys. **40**, 893 (1968).
[80] S. Saito, Prog. Theor. Phys. **41**, 705 (1969).
[81] T. Myo, A. Umeya, K. Horii, H. Toki, and K. Ikeda, Prog. Theor. Exp. Phys. **2014**, 033D01 (2014).
[82] R. B. Wiringa, Steven C. Pieper, J. Carlson, V. R. Pandharipande, Phys. Rev. C **62**, 014001 (2000).
[83] A. A. Ogloblin, A. S. Demyanova, A. N. Danilov, S. V. Dmitriev, T. L. Belyaeva, S. A. Goncharov, V. A. Maslov, Yu. G. Sobolev, W. Trzaska, and S.V. Khlebnikov, EPJ Web Conf. **66**, 02074 (2014).
[84] P. Chevallier, F. Scheibling, G. Goldring, I. Plesser, and M. W. Sachs, Phys. Rev. **160**, 827 (1967).
[85] M. Freer et al., Phys. Rev C **51**, 1682 (1995).
[86] M. Itoh et al., J. Phys.: Conf. Ser. 569, 012009 (2014).
[87] P. Descouvemont and D. Baye, Nucl. Phys. A **573**, 28 (1994).